Monthly Notices
of the
ROYAL ASTRONOMICAL SOCIETY

MNRAS **432,** 327–335 (2013)
Advance Access publication 2013 April 11

doi:10.1093/mnras/stt468

Spectroscopic orbital analysis of the δ Scuti binary, RS Cha – High-resolution spectroscopy reveals a third component

R. M. Woollands,[1,2,3]⋆ K. R. Pollard,[1] D. J. Ramm,[1] D. J. Wright[1,4] and T. Böhm[5,6]

[1]*Department of Physics and Astronomy, University of Canterbury, Private Bag 4800, Christchurch 8140, New Zealand*
[2]*Department of Physics and Astronomy, University of Minnesota – Twin Cities, Minneapolis, MN 55455, USA*
[3]*Department of Aerospace Engineering, Texas A&M University, College Station, TX 77843, USA*
[4]*Department of Astrophysics, School of Physics, University of New South Wales, Sydney, NSW 2052, Australia*
[5]*Université de Toulouse, UPS-OMP, IRAP, F-31000 Toulouse, France*
[6]*CNRS, IRAP, 14 avenue Edouard Belin, F-31400 Toulouse, France*

Accepted 2013 March 13. Received 2013 March 11; in original form 2012 March 18

ABSTRACT

Over the last 40 years variations in the systemic velocity and the observed minus computed time of first conjunction have been observed in the RS Cha binary system. Our goal is to determine the probability for the existence of a third body in this system, and to calculate an orbital solution for this component. A total of 381 high-resolution echelle spectra were obtained at Mount John University Observatory using the 1.0-m McLellan telescope and High Efficiency and Resolution Canterbury University Large Echelle Spectrograph (HERCULES; echelle spectrograph). The spectra were collected during three observing runs occurring over a 15 month period spanning from 2005 November 18 to 2007 February 17, and the data were reduced using the HERCULES reduction software package 2.3. Radial velocities for the 46 echelle orders were generated using Two-Dimensional Correlation, and the velocities from the best 15 orders were selected and used in the calculation of a weighted mean. The weight for each order was determined by generating a preliminary orbital solution for that particular order, using Stern's method, with the rms of the orbital fit used to calculate the associated weight on the order. Systemic velocities for each of the three observing runs were computed by applying a linear regression to the radial velocities of one star against its companion (i.e. V_1 versus V_2). The value of the slope and intercept of the regression line are required for calculating the systemic velocity. Analysis of the 381 spectra confirmed the suspected variation of the system velocity during the time-span over which these data were collected. The systemic velocity for each observing run differs significantly (12.13 ± 0.26, 11.41 ± 0.22 and 9.68 ± 0.78 km s^{-1}) and combined with four historical (previously published) values they failed the χ^2 test, and imply a 99.9 per cent confidence that a third body exists. Three possible orbital solutions for the third body, with respect to the close binary, were generated using the historical and current systemic velocity values ($P = 12.69 \pm 0.01$ or 24.17 ± 0.01 or 74.45 ± 0.02 d). The orbital solution for the binary was calculated after the effects of the shift in systemic velocity during the course of our data were removed. Values for the period and masses are $P = 1.66988 \pm 0.00002$ d, $M_1 = 1.823 \pm 0.012\,\mathrm{M}_\odot$ and $M_2 = 1.764 \pm 0.012\,\mathrm{M}_\odot$, with the lowest possible mass range obtained from the orbital solutions of the third body ranging from $M_3 = 0.30$ to $0.52\,\mathrm{M}_\odot$.

Key words: binaries: close – binaries: eclipsing – binaries: spectroscopic – stars: individual: RS Cha – stars: pre-main-sequence.

1 INTRODUCTION

RS Cha is rare and unique object possessing several fascinating characteristics which may account for the large number and broad nature of studies that have been performed on it to date.

⋆ E-mail: robyn.woollands@gmail.com

In addition to being an eclipsing double-lined spectroscopic binary system (SB2E), a recent study (Böhm et al. 2009) has confirmed that both the Herbig Ae components are undergoing non-radial pulsations, thus allowing both stars in the system to also be classified as δ Scuti-type variable stars.

SB2E systems, like RS Cha, are extremely important and are one of the few ways that astronomers can measure such fundamental stellar parameters as mass and radius. From a photometric orbital solution we can obtain the relative size of the stellar radius to the relative size of the orbit ($R_{1,2}/a$), where $a = a_1 + a_2$, the eccentricity (e), the inclination (i), the period (P) and the ratio of effective temperature ($T_{\rm eff1}/T_{\rm eff2}$). From a double-lined spectroscopic solution we can obtain the radial velocity amplitude ($K_{1,2}$), the eccentricity, the period, the scaled length of the semimajor axis of the orbit ($a_{1,2}\sin i$), and the scaled masses ($M_{1,2}\sin^3 i$). Knowledge of the system's inclination from the photometric solution allows direct measures of the masses, semimajor axes, stellar radii and luminosities to be made.

RS Cha's δ Scuti nature combined with its classification as a Herbig Ae star present an opportunity to study the stellar interior of the young star. This is done using a technique known as asteroseismology that examines pulsation characteristics to infer the inner stellar structure. Both the ability to calculate the stellar masses and radii from a spectroscopic binary study, and to be able to probe the stellar interior using asteroseismology are important tools for determining stellar parameters and refining models of stellar evolution – thus making RS Cha a valued celestial object.

The numerous studies done on RS Cha (HD 75747) have resulted in publication of several well-defined parameters. RS Cha is a relatively bright ($V = 6.05$) southern star whose variability due to eclipses was discovered by Strohmeier (1964). Its spectral type is given as A8V + A8V (Young et al. 2001). The inclination of the system is $83\overset{\circ}{.}4 \pm 0\overset{\circ}{.}3$ and the stars are believed to be in a circular orbit, with an orbital period of 40.07 h (Clausen & Nordstrom 1980). RS Cha has a parallax of 10.77 ± 0.24 mas (van Leeuwen 2007), which corresponds to a distance of 92.9 ± 2.1 pc. It is a member of the η Cha cluster (consisting of about 50 T Tauri stars) and it is believed to be a pre-main-sequence system based on the X-ray emission detected by Mamajek, Lawson & Feigelson (1999). The age has been estimated between 6 and 8 Myr (Mamajek et al. 1999; Luhman & Steeghs 2004).

Two recent spectroscopic studies of RS Cha give values for the orbital elements (Alecian et al. 2005), and discuss the modes of pulsation occurring in the components (Böhm et al. 2009). Alecian et al. (2005) calculated values for the primary and secondary masses and radii as follow: $M_1 = 1.89 \pm 0.01\,{\rm M}_\odot$, $R_1 = 2.15 \pm 0.06\,{\rm R}_\odot$, $M_2 = 1.87 \pm 0.01\,{\rm M}_\odot$, $R_2 = 2.36 \pm 0.06\,{\rm R}_\odot$. Böhm et al. (2009) also performed an orbital analysis, but their focus was directed to determining modes of pulsation. Interestingly, in both papers the analysis mentioned the detection of a slight variation in systemic velocity. However, neither was able to confirm the presence of a third body influencing the system and both suggest that an extensive study based on a larger data set is needed.

The aim of our study is to calculate a probability for the existence of a third body, and subsequently to determine its orbital solution with respect to the binary system. In order to accomplish this goal, high-resolution spectroscopic data were collected at Mount John University Observatory (MJUO) over a period of 15 months, and our findings were then compared with historical data published on this system.

Details regarding the instrumentation, observations and data reduction are presented in Section 2. The method for measuring the radial velocities, and the orbit investigation are discussed in Section 3. The calculation of the orbital solution for the third body, along with the orbital solution for the binary is shown in Section 4. Masses, radii and Roche lobes are discussed in Section 5, and the main ideas and ultimate conclusions are summarized in Section 6.

2 INSTRUMENTS AND OBSERVATIONS

2.1 Mount John University Observatory

Observations of RS Cha were made from the University of Canterbury's MJUO located near Tekapo, New Zealand at $170^\circ 27\overset{'}{.}9$ E, $43^\circ 59\overset{'}{.}2$ S at an elevation of 1029 m above mean sea level. Spectra were obtained using the 1.0-m McLellan telescope and the fibre-fed High Efficiency and Resolution Canterbury University Large Echelle Spectrograph (HERCULES; Hearnshaw et al. 2003), with a spectral resolving power of about $R \sim 45\,000$.

2.2 Spectra

A total of 381 spectra were obtained using the Photometrics Series 200 1 k × 1 k CCD camera system that includes orders 80 (7082 Å) to 126 (4532 Å). In general, a sequence of five or six RS Cha exposures [typical duration of 300–600 s, signal-to-noise ratio (S/N) $\sim$ 100] were followed by a thorium–argon arc calibration exposure. The Julian Date corresponding to each spectrum is automatically calculated by the observing software as the flux-weighted mean time during an observation. To conclude each night of observing three or four smooth fields (typical duration of 1–2.5 s) were taken as these, along with the thorium–argon images, were required for data reduction. Three separate observing runs from 2005 November to 2007 March allowed a total of 27 nights of data to be collected.

2.3 Data reduction and preparation

The spectra were reduced using HRSP, the HERCULES reduction software package, version 2.3 (Skuljan 2004). The thorium–argon spectra mentioned in Section 2.2 are necessary for wavelength calibration and the smooth fields are required for order recognition and tracing. Interpolating the solutions corresponding to each set of thorium–argon images allowed a dispersion solution to be produced which was used for the wavelength calibration. Data reduction culminated with the creation of a one-dimensional spectrum for each order.

After data reduction the corresponding barycentric velocity and Heliocentric Julian date corrections were applied to each observation. Each order of the 381 spectra were then continuum normalized, by fitting a spline to manually selected continuum points, and finally lightly smoothed, by applying a low-pass Fourier filter to eliminate high-frequency noise (i.e. eliminating frequencies higher than $\sim$2 pixels). Out of the 46 available orders the best 15 orders (091, 101, 106-109, 111, 115, 116, 119, 121–125) were selected for measuring stellar radial velocities. These orders contain very little telluric absorption thus resulting in a higher quality normalization and a more precise radial velocity.

3 ORBITAL ANALYSIS

3.1 Radial velocities

Two radial velocities (one each for the primary and secondary components) for every one of the 381 spectra were obtained by

two-dimensional cross-correlation using Two-Dimensional Correlation (TODCOR; Zucker & Mazeh 1994). This algorithm simultaneously determines the Doppler shift of both components in each spectrum by extending the traditional one-dimensional cross-correlation technique, with one template spectrum, to include two different template spectra. In general the two template spectra are unique as they represent the individual spectral types of each star in the system, however, since the RS Cha components are of an identical spectral type, the same template spectrum is used twice. The template spectrum selected was a high S/N spectrum of RS Cha taken on 2006 December 6 when the stars were undergoing an eclipse. A total of 15 sets of the 381 radial velocities were generated for each star.

3.2 Orbital investigation

Typically an orbital analysis using spectroscopic radial velocities assumes that all of the parameters (e.g. K, e, P and the systemic velocity, γ) are constant.[1] However, inspection of the literature relating to RS Cha suggests significant changes to the systemic velocity over time (Chambliss 1969: 26 ± 3 km s^{-1}; Jones 1969: 10.6 ± 1.1 km s^{-1}; Andersen 1975: 15.9 ± 0.5 km s^{-1}; Alecian et al. 2005: 15.7 ± 0.2 km s^{-1}). Since our HERCULES data set is large (more than twice that of any previous data set) and we have three distinct sets of observations spread over 15 months, we could pursue an analysis to determine whether a systemic velocity variation existed within the time span-over which our three data sets were collected.

To begin this analysis it is first necessary to calculate the mean value for the radial velocities from the 15 selected orders. Theoretical studies by Murdoch & Hearnshaw (1991) conclude that factors such as the depth, width and number of absorption lines present in an order, in addition to the S/N, airmass, exposure time and observing conditions, all contribute to impacting the wavelength dependence of the incident light. As a result one would expect the orders to be unequally weighted, and thus it is essential that a weighted mean be calculated.

The weights are determined by employing the orbital fit technique perceived by Ramm (2008), that utilizes Stern's (1941) method for each of the 15 orders of radial velocities, thus endeavouring to achieve the optimal orbital fit. The initial iteration of Stern's method sets all weights as $w = 1$, and an estimate of each orbital element is used based on previously published values (Alecian et al. 2005). The rms error obtained in the final iteration is used to calculate the weight given to that specific order, by $w = 1/\sigma^2$. To date the orbital fit technique has been superior as the best-fitting rms error to the final solution. It reduces the error by approximately 15 per cent than that obtained with all the weights set at the value of $w = 1$ (see Ramm, Skuljan & Hearnshaw 2004; Skuljan, Ramm & Hearnshaw 2004; Ramm 2008).

Once the weighted mean of the 15 sets of radial velocities has been calculated the linear regression of one star's velocities is plotted against its companion's (Fig. 1). The systemic velocity can then be calculated from equation (1), where γ_1 is the systemic velocity, c_1 is the intercept and q_1, the mass ratio, is the absolute value of the slope of the linear regression line. A full derivation for equation (1) is given in Appendix A. This systemic velocity calculation is done

[1] It is assumed that if the systemic velocity is changing, then the other orbital elements such as the eccentricity and the longitude of periastron passage should also change, but these two only change if the orbit is non-circular which is not the case for RS Cha (Wood 1971).

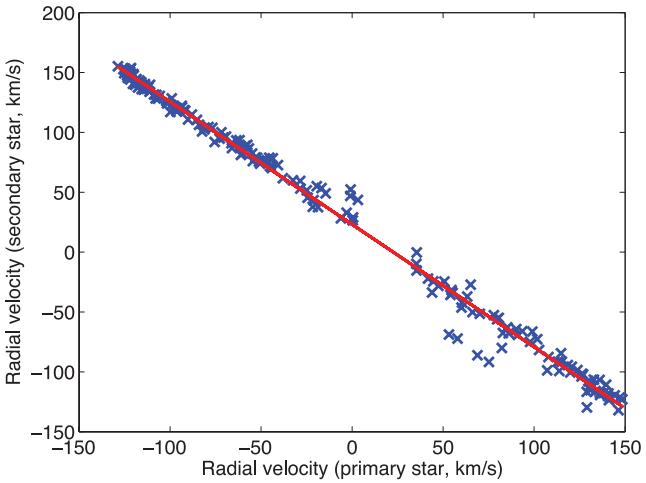

Figure 1. The least-squares fit for the linear regression of the primary and secondary radial velocities. The portion of data shown is for Julian Date ranging between 245 3745.944 and 245 3758.143, corresponding to the second observing run.

Table 1. Published and recalculated systemic velocities.

Paper	Published γ values	Recalculated γ values
Chambliss (1969)	26 ± 3 km s^{-1}	20.20 ± 2.76 km s^{-1}
Jones (1969)	10.6 ± 1.1 km s^{-1}	12.92 ± 1.03 km s^{-1}
Andersen (1975)	15.9 ± 0.5 km s^{-1}	16.78 ± 0.72 km s^{-1}
Alecian et al. (2005)	15.7 ± 0.2 km s^{-1}	–
This paper	–	12.13 ± 0.26 km s^{-1}
This paper	–	11.41 ± 0.22 km s^{-1}
This paper	–	9.68 ± 0.78 km s^{-1}

for both plotting arrangements, i.e. V_1 versus V_2 and V_2 versus V_1, respectively. Using these two values of the systemic velocity, one obtained from each plotting arrangement, a weighted mean is calculated for the data from each of the three subgroups (observing runs) separately in order to determine their individual systemic velocities. These values are displayed in the last three rows of Table 1:

$$\gamma_1 = \frac{c_1}{1 + q_1}. \quad (1)$$

Calculating the systemic velocity in this manner confirmed our suspicion of a perturbed or variable systemic velocity for the RS Cha system. Several factors were considered as possible sources for the detected perturbations to the systemic velocity. These included the existence of a third star in the system, the non-spherical shapes of the stars and a shifting spectrograph zero-point. It is unlikely that the non-spherical shapes of the stars would be the culprit in this instance as the duration of δ Scuti pulsations are substantially shorter than the recognized orbital period (Böhm et al. 2009). The shifting spectrograph zero-point can also be eliminated due to the fact that this condition would be detected in the data collected by other observers using HERCULES. (For further details refer to Komonjinda, Hearnshaw & Ramm 2007, where an rms error of only 16 m s^{-1} was obtained from 142 spectra collected during the course of 5 yr, thus suggesting that HERCULES is incredibly stable.) As a result, the most feasible answer for the variation in the systemic velocity would be the presence of a third body in the system.

In order to broaden the scope of our study, at this point we incorporated all the published values of the systemic velocity for the RS Cha system into our analysis. Several papers have published

values of the systemic velocity, but three of these papers have also published the radial velocity values. Using these radial velocity values the same regression analysis, as that previously described, is performed on these historical data sets. This produces systemic velocities derived in the same manner as ours so that a more valid comparison can be made. We are able to follow this procedure as the velocities in these papers had been heliocentrically corrected and could thus be assumed to share a common zero-point. The published and recalculated systemic velocity values are shown in Table 1. Alecian et al. (2005) did not publish radial velocity values and thus only their published value is shown in the table. Some of the historical values vary considerably from their published values which may be a result of modern computational methods used for this paper.

These seven values for systemic velocity, six in the right column and the one calculated by Alecian et al. (2005) in the middle column, fail the χ^2 test for consistency with a significance of less than 0.001 (equation 2), implying a 99.9 per cent confidence that a third body exists. The χ^2 test is a well established test (Greenwood & Nikulin 1996), and the value of χ^2 is dependent on the uncertainty associated with each systemic velocity, as well as the weighted mean systemic velocity. The uncertainties on the individual systemic velocities are calculated using an algorithm from Numerical Recipes (Press et al. 1992) for a least-squares fit to a straight line. The assumed weighted mean systemic velocity is calculated as $\gamma_{\rm mean} = 13.38 \pm 0.12$ km s^{-1} for the data in Table 1. Refer to Appendix A, equations (A14)– (A19), for more details regarding this calculation:

$$\chi^2 = \sum_{i=1}^{N} \left(\frac{\gamma_i - \gamma_{\rm mean}}{\sigma_i} \right)^2, \qquad (2)$$

where γ_i is the observed systemic velocity, $\gamma_{\rm mean}$ is the expected value and σ_i is the uncertainty in each systemic velocity value.

In the papers by Alecian et al. (2005) and Böhm et al. (2009), the changing time of conjunction (or primary mid-eclipse) is discussed. Alecian et al. (2005) used photometric and spectroscopic observations of RS Cha available in the literature (Jones 1969; Andersen 1975; Clausen & Nordstrom 1980; Mallama 1981), combined with data from the *Hipparcos* and Tycho catalogues to calculate the observed minus computed (O-C) timings of first and second conjunctions (refer to fig. 2 in Alecian et al. 2005).

The error bars for the measurements in fig. 2 of Alecian et al. (2005) are sufficiently small to show that there are significant changes over time to the time of conjunction. This supports our hypothesis that a third body is influencing the time of conjunction and systemic velocity. Both Alecian et al. (2005) and Böhm et al. (2009) noted the appearance of a changing systemic velocity but due to their comparatively small data sets they were unable to confirm the presence of a third body.

We have established that the systemic velocity is shifting, and now to find a possible solution for the orbital period of the third body some more values for the systemic velocity are produced by creating subgroups of the available historical data sets. This is done by dividing each historical data set that has a significant amount of data, and extends over a time-span longer than about 30 d. Thus, the value of systemic velocity calculated for each subgroup represents data that were collected over a time-span of less than 30 d. The new systemic velocities are presented in Table 2.

The Julian Date corresponding to each systemic velocity is calculated as the mean for that data set, with the error calculated as the standard deviation. A graphical representation of the data in Table 2 is displayed in Fig. 2. It is expected that if there is only one other star affecting the systemic velocity, i.e. a triple system, the systemic velocities would vary in a smooth periodic manner.

Table 2. Additional systemic velocities calculated for each subgroup.

Paper	Mean Julian date	New systemic velocity
Chambliss (1969)	243 9582.4 ± 2.1	28.14 ± 2.92 km s^{-1}
	243 9612.9 ± 3.9	5.34 ± 4.11 km s^{-1}
Jones (1969)	243 9634.5 ± 1.1	12.91 ± 1.03 km s^{-1}
	243 9932.7 ± 5.7	13.72 ± 1.20 km s^{-1}
Andersen (1975)	244 1724.4 ± 3.1	17.48 ± 1.51 km s^{-1}
	244 1798.8 ± 2.2	16.27 ± 0.36 km s^{-1}
Alecian et al. (2005)	245 2626.3 ± 0.1	15.7 ± 0.2 km s^{-1}
This paper	245 3703.5 ± 5.7	12.13 ± 0.26 km s^{-1}
This paper	245 3753.4 ± 3.4	11.41 ± 0.22 km s^{-1}
This paper	245 4142.8 ± 5.3	9.68 ± 0.78 km s^{-1}

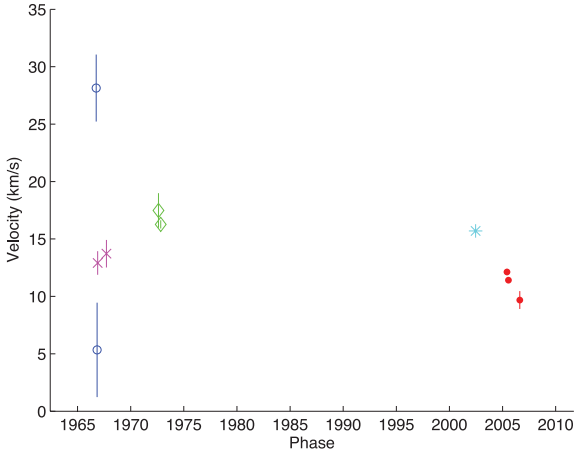

Figure 2. A graphical representation of the systemic velocities shown in Table 2. Open circles: Chambliss (1969); large crosses: Jones (1969); diamonds: Andersen (1975); asterisk: Alecian et al. (2005); full circles: this paper.

4 ORBITAL SOLUTION

4.1 Third body parameters

The period for the third body is determined using an algorithm developed by Mazeh et al. (1987). The algorithm subjects the data to a period search over a desired period range set by the operator, and thus employs a power-series analysis to output the best period in the desired range. In general, a 10 d range was input by the operator and this was shifted forward by 5 d for each successive search. That is, the first range was 1–10 d, the second 5–15 d, the third, 10–20 d and so on. This process was repeated until about 370 d (∼1 yr). There is no need to continue searching for periods beyond this point as we know that the systemic velocity is varying over a shorter time-span than 1 yr, and the errors associated with periods of greater that about 120 d are large (Fig. 3).

After discovering likely periods in the following regions, 12–13, 24–25 and 74–75 d (crosses in Fig. 3), the original 10 d search range was narrowed in order to isolate the optimal period for each of the three specified regions. This period value is then used to obtain an orbital solution iteratively through least-squares minimization. The orbital elements for these three orbital solutions for the third mass (M_3) are given in Table 3, and the phase plots are displayed

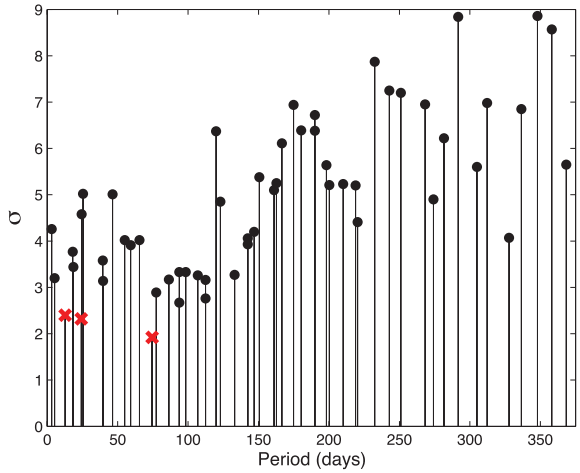

Figure 3. Possible periods for the third body ranging from 1 to about 370 d. Three periods exhibit a σ value of less than 2.5 (large crosses).

in Figs 4–6. The solutions obtained are just a few of many, the reason being that due to only 10 available values of the systemic velocity the solutions are insufficiently well defined. In Table 3 P_3 is the period, γ_3 is the systemic velocity, K_3 is the amplitude of the systemic velocity curve, T is the time of periastron passage, e_3 is the eccentricity, w is the longitude of periastron and f_M, the mass function, is the mass ratio of the secondary to the primary (equation 3):

$$\frac{q^3}{(1+q)^2} = \frac{f_{M_{\rm PS}}}{M_{\rm PS}\sin^3 i}, \tag{3}$$

where $M_{\rm PS} = M_1 + M_2$ and $q = \frac{M_3}{M_{\rm PS}}$.

Although these three orbital fits for the third body are relatively good, as σ is low, these are by no means definitive orbits, since in each case we have assumed M_3. The mass of the third star can be estimated from the mass function $f_{M_{\rm PS}}$, and depends on the inclination of this system, however, a value for M_3 cannot be calculated until the values of M_1 and M_2 are known.

4.2 Binary orbit parameters

The systemic velocity is changing, and thus to determine the binary orbital solution for this system the effects of the change must somehow be minimized or removed. Referring to the three 'best' orbital solutions for the third body, it is clear that there is no simply approached to remove this effect because these approximated functions (solutions) are all so different. One method would be to take the weighted average of the three systemic velocities and apply a 'step' shift to align all the data with the average systemic velocity.

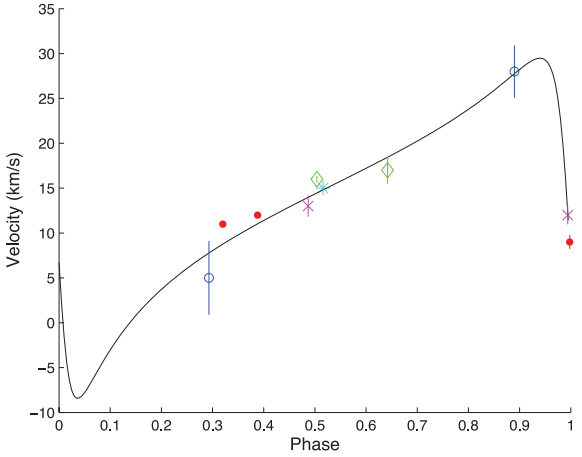

Figure 4. A phase plot (P = 12.69 d) for one of many possible orbital solutions for the third body in the RS Cha system. Open circles: Chambliss (1969); large crosses: Jones (1969); diamonds: Andersen (1975); asterisk: Alecian et al. (2005); full circles: this paper.

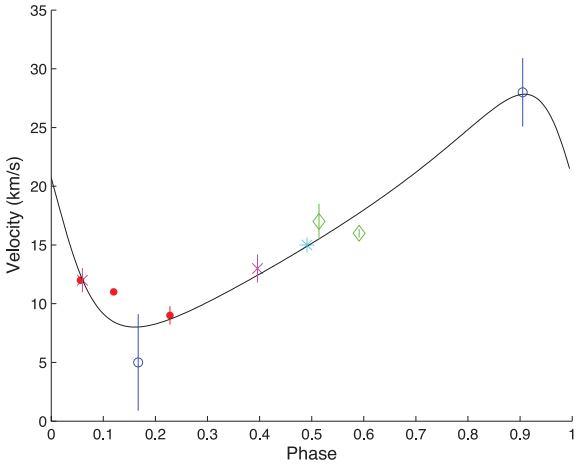

Figure 5. A phase plot (P = 24.17 d) for one of many possible orbital solutions for the third body in the RS Cha system. Open circles: Chambliss (1969); large crosses: Jones (1969); diamonds: Andersen (1975); asterisk: Alecian et al. (2005); full circles: this paper.

Another approach, that is probably less drastic, is to fit a straight line to the three systemic velocities for the data obtained for this paper. The difference between this fitted line and the mean systemic velocity (13.38 ± 0.12 km s^{-1}) is then calculated and subtracted from the radial velocities so that they all share a common zero-point. This is

Table 3. The orbital elements for three possible solutions for the orbit of the third star in the RS Cha system.

Orbital elements	Solution 1	Solution 2	Solution 3
P_3 (d)	12.69 ± 0.01	24.17 ± 0.01	74.45 ± 0.02
γ_3 (km s^{-1})	13.22 ± 10.00	16.77 ± 0.84	15.70 ± 0.81
K_3 (km s^{-1})	18.96 ± 85.14	9.93 ± 1.40	10.44 ± 1.08
T (JD 243 0000)	9583.80 ± 0.82	9584.71 ± 1.64	9582.83 ± 9.93
e_3	0.70 ± 1.76	0.41 ± 0.26	0.18 ± 0.12
w	101.63 ± 99.65	73.83 ± 12.26	369.63 ± 31.68
$f_{M_{\rm PS}}$ ($M_\odot$)	0.0032 ± 0.0457	0.0018 ± 0.0001	0.0084 ± 0.0026
σ	2.19	2.32	1.79

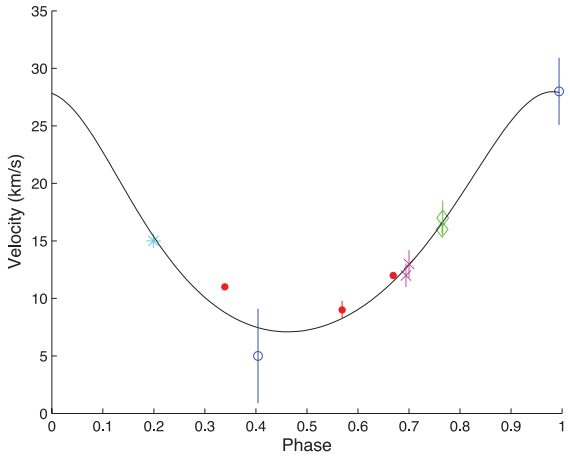

Figure 6. A phase plot ($P = 74.45$ days) for one of many possible orbital solutions for the third body in the RS Cha system. Open circles: Chambliss (1969); large crosses: Jones (1969); diamonds: Andersen (1975); asterisk: Alecian et al. (2005); full circles: this paper.

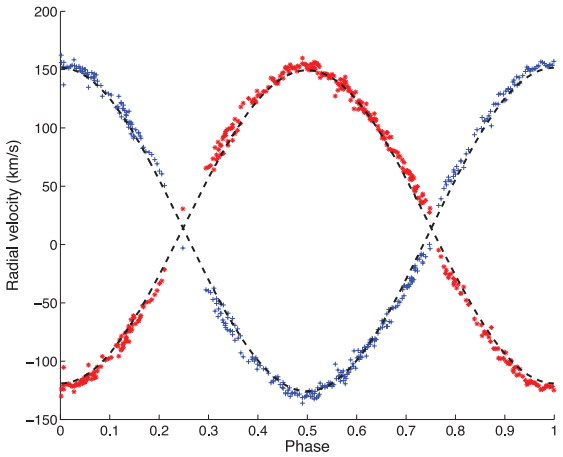

Figure 7. The orbital solution and phase plot for component 1 (cross) and component 2 (star).

the method that we adopted to minimize the shift, thus allowing the respective motion of the binary components alone to be studied.

Ideally, a method that derives orbital solutions for both stars simultaneously is required. For systems that provide velocities for both stars, the recommendations of Jones (1969) have been followed so as to obtain a simultaneous solution for both stars; namely, derive the slope and y-intercept by calculating the linear regression of the velocities, then convert the velocities of the secondary into velocities of the primary and vice versa. Finally, the method of differential corrections of Sterne (1941) was applied to estimate the orbital solution. Two sets of orbital elements are produced, one from the velocities of component 1 and other from component 2. The solution for the system is the weighted mean of these values and is shown in Table 4. The phase plot is shown in Fig. 7.

Using the published value of the inclination ($83\overset{\circ}{.}4 \pm 0\overset{\circ}{.}3$; Clausen & Nordstrom 1980), we derive $a_1 = 2.172 \pm 0.016 \times 10^{-2}$ au, $a_2 = 2.102 \pm 0.016 \times 10^{-2}$ au and $a_1 + a_2 = 4.274 \pm 0.033$ au. Since the orbit is circular, w (longitude of periastron) and T (time of periastron passage) are undefined. Thus the time of periastron passage is replaced by the time of zero mean longitude (T_0; Stern 1941), which is the time of first eclipse.

5 MASSES, RADII AND ROTATIONAL VELOCITIES

5.1 Stellar masses

The masses for the primary and secondary components were calculated using equation (4) (refer to Appendix B for the derivation):

$$M_{1,2} = (1.0361 \times 10^{-7})\, P K_{2,1} (K_1 + K_2)^2 \left[\frac{\sqrt{1-e^2}}{\sin i}\right]^3, \qquad (4)$$

so that $M_1 = 1.823 \pm 0.012\,\mathrm{M}_\odot$ and $M_2 = 1.764 \pm 0.012\,\mathrm{M}_\odot$ for the primary and secondary stellar masses, respectively.

Using these masses ($M_{\mathrm{PS}} = M_1 + M_2$) in equation (3) allows possible values for the mass of the third component to be calculated. Since there is insufficient information to calculate the mass with respect to the derived orbital elements directly, Fig. 8 shows three curves (one for each orbital solution) for the mass ratio as a function of orbital inclination. Referring to Fig. 8, the lowest mass ratios are 0.10 (solution 1), 0.08 (solution 2) and 0.15 (solution 3), which correspond to lower masses of 0.37, 0.30 and 0.52 $\mathrm{M}_\odot$, respectively, for the possible third component if this orbital system has $i = 90^\circ$.

These are realistic values for the mass as they lie close to the mass range of a red dwarf (0.08–0.33 $\mathrm{M}_\odot$) or the mass range of a white dwarf (0.2–1.4 $\mathrm{M}_\odot$). The absolute magnitude range for the third body was calculated as $M_{\mathrm{v}} = 24.96$ (solution 3) to $M_{\mathrm{v}} = 30.32$ (solution 2), using the lowest mass values, respectively. This magnitude range corresponds to that of a red dwarf and explains why the third body is undetectable in the spectrum. Thus it is likely that the third body is a small and faint object, probably a white or red dwarf as these stars are faint, have relatively low mass and are fairly common.

5.2 Stellar radii and Roche lobes

Alecian et al. (2005) published values for the stellar radii in RS Cha as $R_1 = 2.36 \pm 0.06\,\mathrm{R}_\odot$ and $R_2 = 2.15 \pm 0.06\,\mathrm{R}_\odot$, respectively.

Table 4. Binary orbital elements derived for both stellar components assuming a circular orbit. A weighted mean of the period and the systemic velocity, as well as $K = K_1 + K_2$ and $a \sin i = (a_1 + a_2) \sin i$, is displayed in column 4.

Orbital elements	$V_1 = f(V_2)$ solution $n = 1$	$V_2 = f(V_1)$ solution $n = 2$	Adopted solution
P (d)	1.66988 ± 0.00001	1.66988 ± 0.00001	1.66988 ± 0.00001
γ (km s^{-1})	14.07 ± 0.24	14.02 ± 0.24	14.05 ± 0.17
K_n (km s^{-1})	138.68 ± 0.32	134.24 ± 0.32	272.92 ± 0.64
T_0 (JD 245 3000)	752.170 ± 0.001	752.170 ± 0.001	752.170 ± 0.001
$a_n \sin i$ (Gm)	3.1844 ± 0.0073	3.0825 ± 0.0074	6.2669 ± 0.0147

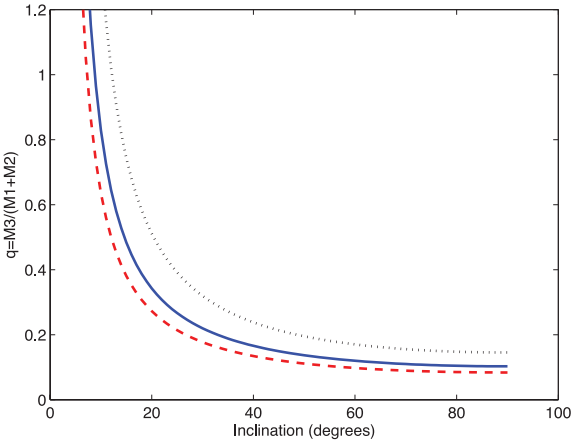

Figure 8. The curves represent possible values for the third mass that depend on the orbital inclination of the third body with respect to the inclination of the binary. The solid line corresponds to solution 1, the dashed line to solution 2, and the dotted line to solution 3.

To determine whether these stars are interacting it is necessary to determine the size of their Roche lobe in relation to their volume. The Roche lobe is the region surrounding each star in a binary system, within which any material is gravitationally bound to that particular star. Using equation (5) (Eggleton 1983) the radius of the Roche lobe can be estimated to an accuracy of about 99 per cent, thus allowing the likeliness of stellar interaction to be determined:

$$r_{\rm L} = \frac{R_{\rm L}}{a} = \frac{0.49 q_{\rm L}^{2/3}}{0.6 q_{\rm L}^{2/3} + \ln(1 + q_{\rm L}^{1/3})}, \tag{5}$$

where $r_{\rm L}$ is the radius of a sphere with the same volume as the Roche lobe (effective volume or radius), relative to the component separation a, $R_{\rm L}$ is the actual effective radius, and the mass ratio is given by $q_{\rm L} = \frac{M_{\rm L}}{M_{\rm C}}$. $M_{\rm L}$ is the mass of the component whose effective radius is calculated and $M_{\rm C}$ is the companion.

Performing this calculation using our values of $q = \frac{M_2}{M_1} = \frac{K_1}{K_2} = 0.97$ showed that the effective radius of the Roche lobe for the primary and secondary components are $r_{\rm L_1} = 0.38$ and $r_{\rm L_2} = 0.37$, respectively. Since $a = 4.189 \pm 0.009 \times 10^{-2}$ au $\equiv 9\,{\rm R}_\odot$, $R_{\rm L} \sim 3.4\,{\rm R}_\odot$. This reveals that both radii are presently about 2/3 the size of each Roche lobe and it is unlikely that matter transfer is occurring in this system. This conclusion is also supported by Mamajek & Feigelson (2001).

5.3 Stellar rotational velocities

The broadening of a spectral line is dependent on the rotational velocity of a star. Although other mechanisms such as pressure broadening, natural broadening and Doppler broadening also contribute to the equivalent width of an absorption/emission line, they are typically small compared with the broadening caused by rotation. As a result these effects have been ignored in the rotational velocity calculation.

Both stars in the RS Cha system exhibit non-radial pulsations and thus it is necessary to first create a representative (average) line profile that minimizes the effects of the non-radial pulsations. The absorption line at 4957.6 Å, in order 115, is well defined and uncontaminated by neighbouring spectral lines. This portion of the spectrum was selected from all the spectra where the individual stellar components were well separated, thus also preventing contamination from the corresponding line of the other star.

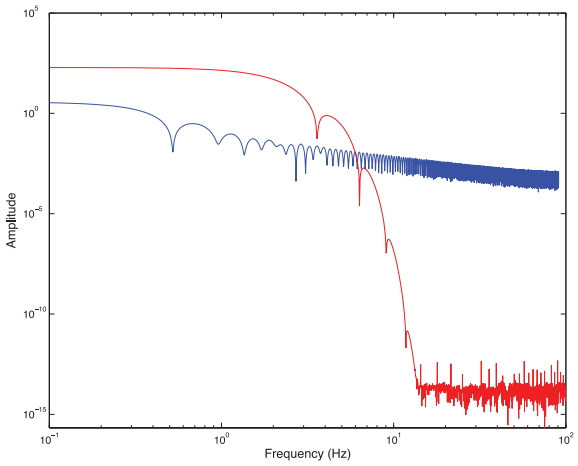

Figure 9. Fourier transforms of the representative RS Cha line profile (large amplitude range) and the theoretically produced line profile ($v \sin i = 10$ km s^{-1}). The ratio of the first minima along the abscissa is equal to the inverse ratio of the rotational velocities, respectively.

A total of 235 high S/N spectra were selected and averaged to create one representative profile for each star. To determine the stellar rotational velocities, the Fourier transform of the representative line profile for each of the stars is computed (Fig. 9). The position of the first minimum along the abscissa is compared with the position of the first minima for the Fourier transform of a theoretically produced line profile (Gray 1992) with $v \sin i = 10$ km s^{-1}. The ratio of these positions is equal to the inverse of the ratio of the rotational velocities and is calculated using equation (6):

$$\frac{v \sin i}{10\,{\rm km\,s^{-1}}} = \frac{x}{y}, \tag{6}$$

where x and y are the positions of the first minima along the abscissa for the theoretical Fourier transform and the representative RS Cha line profile Fourier transform, respectively.

The values of $v_1 \sin i$ and $v_2 \sin i$ are 68 ± 2 and 72 ± 2 km s^{-1}, respectively, and agree with the values of 64 ± 6 and 70 ± 6 km s^{-1} reported by Alecian et al. (2005).

5.4 Synchronization

A binary system is synchronized when the rotation period and the orbital period are the same, or the ratio of the orbital velocities of the two stars is equal to the ratio of their radii (Alecian et al. 2005). These ratios are calculated as follows:

$$\frac{v_1}{v_2} = \frac{R_1}{R_2}, \tag{7}$$

where v_1 and v_2 are the rotational velocities of components 1 and 2, respectively, and R_1 and R_2 are their radii. The ratio of the rotational velocities ($v \sin i$) of the components in this system is 0.95 ± 0.05, and the ratio of their radii is 0.91 ± 0.05. These ratio values agree within the specified uncertainty and thus imply that the system is synchronized.

6 CONCLUSIONS

RS Cha is an eclipsing doubled-lined spectroscopic binary system with both components exhibiting non-radial pulsations (Alecian et al. 2006; Böhm et al. 2009). This combination of characteristics makes it a rare and unique celestial object that has been the focus

of a number of complex studies. Over the last 40 years variations in the systemic velocity and the observed minus computed time of first conjunction have been observed in the system. With good access to a high-resolution echelle spectrograph we undertook an investigation to determine the probability for the existence of a third body, and to compute its orbital solution with respect to the binary system.

A total of 381 high-resolution echelle spectra were obtained at MJUO using the 1.0-m McLellan telescope and HERCULES (echelle spectrograph). The spectra were collected during three observing runs occurring over a 15 month period spanning from 2005 November 18 to 2007 February 17, and the data were reduced using the HERCULES Reduction Software Package 2.3 (Skuljan 2004).

Radial velocities for the 46 echelle orders were generated using TODCOR (Zucker & Mazeh 1994), and the velocities from the best 15 orders were selected and used in the calculation of a weighted mean. The weight for each order was determined by generating a preliminary orbital solution for that particular order, using Stern's (1941) method, with the rms of the orbital fit used to calculate the associated weight on the order. Systemic velocities for each of the three observing runs were computed using a linear regression technique, whereby the radial velocities of each component were plotted against each other (i.e. V_1 versus V_2). The value of slope and intercept of the regression line are required for calculating the systemic velocity.

Analysis of the 381 spectra confirmed the suspected variation of the system velocity during the time-span over which these data were collected. The systemic velocity for each observing run differs significantly (12.13 ± 0.26, 11.41 ± 0.22 and 9.68 ± 0.78 km s^{-1}) and when combined with four historical (previously published) values they failed the χ^2 test, and imply a 99.9 per cent confidence that a third body exists.

Three possible orbital solutions for the third body, with respect to the close binary, were generated using the historical and current systemic velocity values ($P = 12.69 \pm 0.01$ or 24.17 ± 0.01 or 74.45 ± 0.02 d). The orbital solution for the binary was calculated after the effects of the shift in systemic velocity during the course of our data were removed. Values for the period and masses are $P = 1.66988 \pm 0.00002$ d, $M_1 = 1.823 \pm 0.012\,\mathrm{M}_\odot$ and $M_2 = 1.764 \pm 0.012\,\mathrm{M}_\odot$, with the lowest possible mass range obtained from the orbital solutions of the third body ranging from $M_3 = 0.30$ to $0.52\,\mathrm{M}_\odot$.

In addition, calculations regarding the stellar Roche lobes, stellar rotational velocities and system synchronization were completed. The Roche lobe computation revealed that both stars currently fill only 2/3 of their respective Roche lobe, thus confirming Alecian et al. (2005)'s statement that no matter transfer is occurring in this system. The stellar rotational velocities of the binary components were calculated to be $v_1 = 68 \pm 2$ km s^{-1} and $v_2 = 72 \pm 2$ km s^{-1}, which agree with the respective values published by Alecian et al. 2005 ($v_1 = 64 \pm 6$ km s^{-1} and $v_2 = 70 \pm 6$ km s^{-1}). Finally, the ratio of the rotational velocities and the ratio of the radii were compared and were found to be in agreement, thus confirming a synchronized system (Alecian et al. 2005).

ACKNOWLEDGEMENTS

The authors would like to thank Pam Kilmartin (University of Canterbury, UC) for completing the final observing run, Siramas Komonjinda (UC) for her advice regarding TODCOR and John Hearnshaw (UC), Peter Cottrell (UC), Alan Gilmore (UC), Michael Albrow (UC) and Ed Guinan (Villanova University) for their general advice and discussion regarding this research. Andrea Woollands also deserves a special mention, we thank her for all the time that she donated to help with spectrum continuum fitting.

RMW would also like to acknowledge financial support received in the form of scholarships from the University of Canterbury's Department of Physics and Astronomy, and the Dennis William Moore Fund. Thanks also need to be extended to the International Astronomical Union, Angkasa Malaysia, the Universiti Kebangsaam Malaysia, the University of Malaya, the Frank Bradshaw and Elizabeth Pepper Wood Fund and the Kingdon-Tomlinson Fund administered by the Royal Astronomical Society of New Zealand, for their respective financial contributions that enabled RMW to participate and present parts of this work at the 29th International School for Young Astronomers (2007) and Astronomical Society of Australia meeting (2007).

REFERENCES

Alecian E., Catala C., Veer-Mennerent C. V., Goupil M.-J., Balona L., 2005, A&A, 442, 993
Alecian E., Catala C., Goupil M. J., Lebreton Y., Dupret M. A., 2006, Mem. Soc. Astron. Ital., 77, 93
Andersen J., 1975, A&A, 44, 445
Böhm T., Zima W., Catala C., Alecian E., Pollard K., Wright D., 2009, A&A, 497, 183
Chambliss C. R., 1969, MNRAS, 142, 113
Clausen J., Nordstrom B., 1980, A&A, 83, 339
Eggleton P. P., 1983, ApJ, 268, 368
Gray D. F., 1992, The Observation and Analysis of Stellar Photospheres. Cambridge Univ. Press, Cambridge
Greenwood P. E., Nikulin M. S., 1996, A Guide to Chi-Squared Testing. Wiley, New York
Hearnshaw J. B., Barnes S. I., Frost N., Kershaw G. M., Graham G., Nankivell G. R., 2003, in Ikeuchi S., Hearnshaw J., Hanawa T., eds, ASP Conf. Ser. Vol. 289, IAU 8th Asian-Pacific Regional Meeting. Astron. Soc. Pac., San Francisco, p. 11
Jones D., 1969, Mon. Notes Astron. Soc. South Africa, 28, 5
Komonjinda S., Hearnshaw J. B., Ramm D. J., 2007, in Hartkopf W. I., Guinan E. F., Harmanec P., eds, Proc. IAU Symp. 240, Binary Stars as Critical Tools and Tests in Contemporary Astrophysics. Cambridge Univ. Press, Cambridge, p. 531
Luhman K., Steeghs D., 2004, ApJ, 609, 917
Mallama A. D., 1981, PASP, 93, 774
Mamajek E. E., Feigelson E. D., 2001, in Jayawardhana R., Greene T., eds, ASP Conf. Ser. Vol. 244, Young Stars Near Earth: Progress and Prospects. Astron. Soc. Pac., San Francisco, p. 104
Mamajek E. E., Lawson W. A., Feigelson E. D., 1999, ApJ, 516, L77
Mazeh T., Kemp J. C., Leibowitz E. M., Meningher H., Mendelson H., 1987, ApJ, 317, 824
Murdoch K., Hearnshaw J. B., 1991, Ap&SS, 186, 169
Press W. H., Teukolsky S. A., Vetterling W. T., Flannery B. P., 1992, Numerical Recipes in C. The Art of Scientific Computing. Cambridge Univ. Press, Cambridge
Ramm D. J., 2008, MNRAS, 387, 220
Ramm D. J., Skuljan J., Hearnshaw J. B., 2004, Observatory, 124, 167
Skuljan J., 2004, in Kurtz D. W., Pollard K. R., eds, ASP Conf. Ser. Vol. 310, Proc. IAU Colloq. 193, Variable Stars in the Local Group. Astron. Soc. Pac., San Francisco, p. 575
Skuljan J., Ramm D. J., Hearnshaw J. B., 2004, MNRAS, 352, 975
Stern T. E., 1941, Proc. Natl. Acad. Sci. USA, 27, 175
Strohmeier W., 1964, Inf. Bull. Var. Stars, 55
van Leeuwen F., 2007, A&A, 474, 2
Wood D., 1971, ApJ, 76, 701
Young P. A., Mamajek E. E., Arnett D., Liebert J., 2001, ApJ, 556, 230
Zucker S., Mazeh T., 1994, ApJ, 420, 806

APPENDIX A: RADIAL VELOCITY EQUATIONS

The radial velocity equations for the primary and secondary stars are, respectively,

$$V_1 = \gamma - \frac{q}{1+q} K(e\cos w + \cos(v+w)) \tag{A1}$$

and

$$V_2 = \gamma + \frac{1}{1+q} K(e\cos w + \cos(v+w)), \tag{A2}$$

where K is the semi-amplitude of the relative orbit, w is the position angle of periastron passage, v is the orbital true anomaly, $q = M_2/M_1$ is the mass ratio, γ is the systemic velocity and $V_{1,2}$ is the radial velocity. Then

$$(V_2\, q) + V_1 \tag{A3}$$

gives

$$V_1 = -q V_2 + (1+q)\gamma \tag{A4}$$

and

$$V_2 = -\frac{1}{q} V_1 + \left(\frac{1+q}{q}\right)\gamma. \tag{A5}$$

Each of these represents straight lines in terms of V_1 and V_2.

For equation (A4) the intercept is given by

$$c_1 = (1+q_1)\gamma_1, \tag{A6}$$

where the slope is

$$s_1 = -q \tag{A7}$$

and γ_1 is

$$\gamma_1 = \frac{c_1}{1+q_1}. \tag{A8}$$

For equation (A5) the intercept is given by

$$c_2 = \left(\frac{1+q_2}{q_2}\right)\gamma_2, \tag{A9}$$

where the slope is

$$s_2 = -\frac{1}{q} \tag{A10}$$

and γ_2 is

$$\gamma_2 = \left(\frac{q_2}{1+q_2}\right) c_2. \tag{A11}$$

The uncertainty in q_1 and q_2 is given by

$$\sigma_{q_1} = \sigma_{s_1} \tag{A12}$$

and

$$\sigma_{q_2} = q_2 \left(\frac{\sigma_{s_2}}{s_2}\right). \tag{A13}$$

The uncertainty in γ_1 and γ_2 is given by the following equations:

$$\sigma_{\gamma_1} = \gamma_1 \sqrt{\left(\frac{\sigma_{c_1}}{c_1}\right)^2 + \left(\frac{q_1}{1+q_1}\right)^2 \left(\frac{\sigma_{q_1}}{q_1}\right)^2} \tag{A14}$$

and

$$\sigma_{\gamma_2} = \gamma_2 \sqrt{\left(\frac{\sigma_{c_2}}{c_2}\right)^2 + \left(\frac{q_2}{1+q_2}\right)^2 \left(\frac{\sigma_{q_2}}{q_2}\right)^2}. \tag{A15}$$

The weighted mean of γ_1 and γ_2 is given by the following equations:

$$G_{\rm w} = \left(\frac{w_1}{w_1+w_2}\right)\gamma_1 + \left(\frac{w_2}{w_1+w_2}\right)\gamma_2, \tag{A16}$$

where

$$w_1 = \frac{1}{\sigma_{\gamma_1}^2} \tag{A17}$$

and

$$w_2 = \frac{1}{\sigma_{\gamma_2}^2}. \tag{A18}$$

The error in $G_{\rm w}$, the weighted mean, is given by the following equation:

$$\frac{1}{\sigma_{G_{\rm w}}^2} = \frac{1}{\sigma_{\gamma_1}^2} + \frac{1}{\sigma_{\gamma_2}^2}. \tag{A19}$$

APPENDIX B: MASS-RELATED EQUATIONS

The mass ratio q is defined by

$$q = \frac{M_2}{M_1} = \frac{K_1}{K_2}, \tag{B1}$$

where

$$K_n = \frac{2\pi}{P}\frac{a_n \sin i}{\sqrt{1-e^2}} \quad \text{for } n = 1, 2 \tag{B2}$$

and

$$K = K_1 + K_2. \tag{B3}$$

From Kepler's 3rd Law:

$$M_1 + M_2 = M_{1,2}\frac{K}{K_{1,2}} = \frac{a^3}{P^2}. \tag{B4}$$

Then

$$M_{1,2} = \frac{K_{2,1}}{K}\left[\frac{K P\sqrt{1-e^2}}{2\pi \sin i}\right]^3 \frac{1}{P^2}, \tag{B5}$$

leading to

$$M_{1,2} = P K_{2,1}(K_1+K_2)^2 \left[\frac{\sqrt{1-e^2}}{2\pi \sin i}\right]^3. \tag{B6}$$

For P in d, K in km s^{-1}, M in M$_\odot$ and i in degrees,

$$M_{1,2} = (1.0361\times 10^{-7}) P K_{2,1}(K_1+K_2)^2 \left[\frac{\sqrt{1-e^2}}{\sin i}\right]^3. \tag{B7}$$

Also by inverting and rearranging equation (B4),

$$\left(\frac{M_2}{M_1+M_2}\right)^2 = \left(\frac{K_1}{K}\right)^2, \tag{B8}$$

and multiplying the respective sides of equation (B8) for the secondary star, we can derive

$$f_{M_1} = \frac{(M_2 \sin i)^3}{(M_1+M_2)^2} = (1.0361\times 10^{-7}) P K_1^3 (1-e)^{2/3}, \tag{B9}$$

where f_{M_1} is known as the mass function corresponding to the primary mass.

This paper has been typeset from a TEX/LATEX file prepared by the author.